Originally published as:

Three-frequency BDS precise point positioning ambiguity resolution based on raw observables

Pan Li[1,2], Xiaohong Zhang* [1,3,4], Maorong Ge[2], Harald Schuh[2]

[1] School of Geodesy and Geomatics (SGG), Wuhan University, Wuhan, China
[2] German Research Centre for Geosciences (GFZ), Telegrafenberg, Potsdam, Germany
[3] Key Laboratory of Geospace Environment and Geodesy, Ministry of Education, Wuhan, China
[4] Collaborative Innovation Center for Geospatial Technology, Wuhan, China

Abstract: All Beidou navigation satellite system (BDS) satellites are transmitting signals on three frequencies, which brings new opportunity and challenges for high-accuracy precise point positioning (PPP) with ambiguity resolution (AR). This paper proposes an effective uncalibrated phase delay (UPD) estimation and AR strategy which is based on a raw PPP model. First, triple-frequency raw PPP models are developed. The observation model and stochastic model are designed and extended to accommodate the third frequency. Then, the UPD is parameterized in raw frequency form while estimated with the high-precision and low-noise integer linear combination of float ambiguity which are derived by ambiguity de-correlation. Third, with UPD corrected, the LAMBDA method is used for resolving full or partial ambiguities which can be fixed. This method can be easily and flexibly extended for dual-, triple-, or even more frequency. To verify the effectiveness and performance of triple-frequency PPP AR, tests with real BDS data from 90 stations lasting for 21 days were performed in static mode. Data were processed with three strategies: BDS triple-frequency ambiguity-float PPP, BDS triple-frequency PPP with dual-frequency (B1/B2) and three-frequency AR, respectively. Numerous experimental results showed that compared with the ambiguity-float solution, the performance in terms of convergence time and positioning biases can be significantly improved by AR. Among three groups of solutions, the triple-frequency PPP AR achieved the best performance. Compared with dual-frequency AR, additional the third frequency could apparently improve the position estimations during the initialization phase and under constraint environments when the dual-frequency PPP AR is limited by few satellite numbers.

Keywords: BeiDou; precise point positioning; triple-frequency ambiguity resolution; raw observable model

1 Introduction

Carrier-phase-based precise point positioning (PPP) has attracted lots of attentions from the Global Navigation Satellite Systems (GNSS) community due to its high computational efficiency, low cost and so on (Kouba and Héroux 2001; Zumberge et al. 1997). A higher positioning performance can be produced with the integer property

of carrier-phase ambiguity considered, compared with the ambiguity-float PPP (Collins et al. 2008; Ge et al. 2008; Laurichesse et al. 2009). The traditional PPP ambiguity resolution (AR) involves the dual-frequency ionosphere-free (IF) GPS observations. Recently achievements have also been gained in the fields of dual-frequency PPP AR with single or combined Beidou navigation satellite system (BDS) and GLONASS system (Banville 2016; Li et al. 2017b; Geng and Shi 2017).

With the rapid development of the new generations of GNSS, GNSS users would be allowed to make use of observations operated on three or more frequencies. The extra frequencies are expected to benefit precise GNSS data processing, such as carrier phase multipath extraction, cycle slip processing (deLacy et al. 2012; Simsky 2006; Zhang and Li 2016), and especially AR. Large number of publications has contributed to the three carrier phase ambiguity resolution (TCAR) for precise relative positioning (e.g., Forssell et al. 1997; Li et al. 2010; Zhang and He 2016). Teunissen et al. (2002) compared the TCAR, cascading integer resolution and the least-squares ambiguity decorrelation adjustment (LAMBDA) methods at different levels, demonstrating LAMBDA the optimal method for GNSS AR. Nevertheless, only a few studies relate to multi-frequency PPP, especially with AR.

As part of the modernization of GPS, newly launched Block-IIF satellites are now transmitting the third civil signal L5 (1176.45 MHz) in addition to the existing L1 (1575.42 MHz) and L2 (1227.60 MHz) signals (http://www.gps.gov). Elsobeiey (2015) chose nine triple-frequency linear combinations based on different criteria, for processing the modernised L5 signal with four Block IIF satellites. It was shown that triple-frequency combinations could improve the PPP convergence time and the precision of the estimated parameters by about 10%. Deo and El-Mowafy (2016) presented three triple-frequency PPP models, namely, the triple-frequency code-only and phase-only ionosphere-free model, the mixed code and phase model and the individual uncombined model. By comparison with the traditional dual-frequency model, it was shown that all three triple-frequency models had improved the convergence time (CT) required to achieve and maintain a 3D positional accuracy of 5 cm, by 8%-11%. The positioning accuracy after convergence for all triple-frequency algorithms was similar and showed marginal improvement. Pan et al (2017) analysed the inter-frequency clock bias (IFCB) for GPS Block IIF satellites and proposed a triple-frequency PPP model that takes the IFCB into account. Their results shown that compared with L1/L2-based PPP, the triple-frequency PPP improved the positioning accuracy by 19, 13 and 21% in the east, north and up coordinate components, respectively.

In order to reduce the initial observation period for successful AR, Geng and Bock (2013) proposed a method where the simulated triple-frequency GPS signals were exploited to enable rapid convergence to ambiguity-fixed solutions in real-time PPP. The extra-wide-lane (EWL), wide-lane (WL) and the narrow-lane (NL) ambiguities were fixed sequentially. Their results showed that the correctness rate of NL AR achieved 99% within 65 seconds, in contrast to only 64% within 150 seconds in dual-frequency PPP. The real performance of triple-frequency PPP AR and their methods should be further assessed with real observations. In addition, for the cases

with more than three frequency observables, their EWL-WL-NL AR strategy must be extended in order to take full advantage of the multi-frequency observables.

BDS is the first satellite constellation in which all satellites transmit triple-frequency signals. The frequencies are 1,561.098 MHz (B1), 1,207.14 MHz (B2) and 1,268.52 MHz (B3). The B1 band is close to the GPS L1 frequency of 1,575.42 MHz, and the B3 band is close to the Galileo E6 with 1,278.52 MHz. The B2 frequency is identical to Galileo E5b. The Chinese BDS launched its regional navigation service in 2012 and has continued its development toward a global system in the near future (http://en.beidou.gov.cn/). Currently (June 1, 2017), the observations from Beidou-3 satellites launched after 2015 are still not available. A total of 14 BDS satellites have been in operation, including five geostationary orbits (GEO), six inclined geosynchronous orbits (IGSO), and three medium altitude Earth orbits (MEO). The BDS provides us a good opportunity to evaluate the performance of triple-frequency PPP AR using real data.

Guo et al. (2016) proposed two kinds of popular ionosphere-free combination and an undifferenced and uncombined PPP model including the functional and stochastic model for BDS triple-frequency observations. By PPP tests performed in both static and kinematic scenarios with real triple-frequency data, they demonstrated that the three triple-frequency PPP models agree well with each other. Additional frequency has a marginal effect on the positioning accuracy in static PPP tests. However, the benefits of the third frequency are significant in situations of where there is poor tracking and contaminated observations on frequencies B1 and B2 in kinematic PPP tests. Only ambiguity-float triple-frequency PPP model and performance are studies in their research.

Gu et al. (2015) conducted triple-frequency ambiguity-fixed PPP based on real tracking BDS data. The EWL and WL ambiguity subsets were formed based on the raw ambiguity estimates and were then fixed with integer least-squares, whereas the BDS L1 ambiguities were kept as float values. Based on two experiments with a typical inter-station distance of 400 and 800 km between the reference stations, it was shown that the EWL and WL AR can obviously improve the PPP in terms of both precision and convergence. In their study, fixing L1 ambiguities was still a difficult task, especially for a network with wide range. The sequential EWL-WL-L1 fixing strategy should be extended for PPP AR with more than three frequencies.

The above reviews reveal that with the new modernized satellites' capabilities, performing PPP with triple-frequency measurements will be possible and the current dual-frequency formulation will not be applicable to the multi-frequency case. There is also a need for a generalized formulation of multi-frequency ambiguity-float and ambiguity-fixed PPP. However, only the initial studying on the triple-frequency PPP AR have been given by Geng et al. (2013) and Gu et al. (2015).

This study aims at proposing a unified UPD estimation and PPP AR method suitable for dual-, triple- and multi- frequency data processing based on raw GNSS model. The UPDs on each frequency are directly estimated from the raw float ambiguities derived with both dual- and three- frequency observables and can be used for resolving full or partial ambiguity sets easiest to be fixed. With the

triple-frequency BDS observables provided by IGS-MGEX, the performance of the triple-frequency PPP AR is also assessed.

This paper is organized as follows: Section 2 formulates the observation equations and stochastic models for PPP based on raw frequency, addresses the methods applied to BDS three-frequency UPD estimation and PPP AR; Section 3 describes the PPP AR processing strategy and experiment scenarios, analyses the performance of triple-frequency PPP AR in terms of the positioning accuracy and the convergence time with comparison with those of triple-frequency ambiguity-float and B1/B2 ambiguity-fixed PPP solutions. Finally, Section 4 presents the conclusions and perspectives.

2 Method

Starting with the basic BDS triple-frequency observational equations, a detailed description of our UPD estimation and PPP AR method are given.

2.1 Observation equations

For a satellite s observed by receiver r, the raw observation of pseudorange P and carrier phase L can be expressed as:

$$P_{r,i}^s = \rho_r^s + c\left(t_r - t^s\right) + \gamma_i \cdot I_{r,1}^s + m \cdot zwd_r + b_{r,i} - b_i^s + e_{r,i}^s \tag{1}$$

$$L_{r,i}^s = \rho_r^s + c\left(t_r - t^s\right) - \gamma_i \cdot I_{r,1}^s + m \cdot zwd_r + \lambda_i \cdot \left(N_{r,i}^s + B_{r,i} - B_i^s\right) + \varepsilon_{r,i}^s \tag{2}$$

where $i = 1,2,3$ refers to the carrier frequency; ρ is the geometric distance between the phase centers of the satellite and receiver antennas; c is the speed of light in vacuum; t_r and t^s are the clock errors of receiver and satellite, respectively; $\gamma_i = f_1^2 \big/ f_i^2$ is the ionospheric factor at frequency i and f is the frequency; $I_{r,1}^s$ is the slant ionospheric delay at B1 frequency; zwd_r is the wet troposphere delay (ZWD) at zenith; $b_{r,i}$ and b_i^s is the code hardware delay from receiver and satellite; e is the pseudorange measurement noise; λ_i is the carrier phase wavelength; $N_{r,i}^s$ is the integer carrier phase ambiguity; $B_{r,i}$ and B_i^s are the receiver-dependent and satellite-dependent carrier phase hardware delay, respectively; and ε is the measurement noise of the carrier phase. Other error items, such as the phase centre offset (PCO) and variation (PCV), dry slant troposphere delay, phase wind-up (Wu et al. 1993), relativistic effect, tide loading, and so on, are assumed to be precisely

corrected with their corresponding models (Petit and Luzum, 2010). Noted that there is no precise PCO/PCV information provided currently for B3 frequency, the PCO/PCV corrections for B2 are used for B3 due to the adjacent frequency for B2 and B3.

Unlike the IF-based PPP models, the slant ionospheric delays should be treated as unknowns in raw PPP. We normally do not estimate hardware biases. Consequently the pseudorange hardware delay biases are lumped into other parameters (ionosphere and receiver clock bias) and the carrier phase hardware delay biases are absorbed by integer ambiguity parameter in the PPP software (Chen et al. 2015; Guo et al. 2015). The same re-parameterization of B1/B2 pseudorange hardware delay biases and ionosphere is employed for triple-frequency PPP. As for the triple-frequency PPP, the hardware biases on the B3 pseudorange, however, cannot be completely absorbed into the ionospheric estimate which has been lumped with the differential code biases between B1 and B2 pseudoranges. An additional IFB parameter is, therefore, required to compensate for these effects.

In addition, the availability of precise reference satellite orbit and clock products from IGS or its analysis centre using a network of GNSS reference stations distributed worldwide is required to fix the satellite clock and orbit in PPP. Following the current IGS analysis convention, the dual-frequency IF pseudorange and carrier-phase with P1 and P2 signals are employed to estimate the precise clock corrections. For GNSS observations, the pseudorange IF hardware delay biases at the satellite side are assimilated into the clock offset $c \cdot t^s$. Therefore, after applying precise satellite clocks, eventually, the linearized observation equations can be written as:

$$P_{r,1}^s = \overline{\rho}_r^s + c \cdot \overline{t}_r + \gamma_1 \cdot \overline{I}_{r,1}^s + m_r^s \cdot zwd_r + e_{r,1}^s \tag{3}$$

$$P_{r,2}^s = \overline{\rho}_r^s + c \cdot \overline{t}_r + \gamma_2 \cdot \overline{I}_{r,1}^s + m_r^s \cdot zwd_r + e_{r,2}^s \tag{4}$$

$$P_{r,3}^s = \overline{\rho}_r^s + c \cdot \overline{t}_r + \gamma_3 \cdot \overline{I}_{r,1}^s + m_r^s \cdot zwd_r + IFB_r^s + e_{r,3}^s \tag{5}$$

$$L_{r,1}^s = \overline{\rho}_r^s + c \cdot \overline{t}_r - \gamma_1 \cdot \overline{I}_{r,1}^s + m_r^s \cdot zwd_r + \lambda_1 \cdot \overline{N}_{r,1}^s + \varepsilon_{r,1}^s \tag{6}$$

$$L_{r,2}^s = \overline{\rho}_r^s + c \cdot \overline{t}_r - \gamma_2 \cdot \overline{I}_{r,1}^s + m_r^s \cdot zwd_r + \lambda_2 \cdot \overline{N}_{r,2}^s + \varepsilon_{r,2}^s \tag{7}$$

$$L_{r,3}^s = \overline{\rho}_r^s + c \cdot \overline{t}_r - \gamma_3 \cdot \overline{I}_{r,1}^s + m_r^s \cdot zwd_r + \lambda_3 \cdot \overline{N}_{r,3}^s + \varepsilon_{r,3}^s \tag{8}$$

with

$$\begin{cases} \bar{I}_{r,1}^s = I_{r,1}^s - \beta_{12}\left(DCB_{r,12} - DCB_{12}^s\right) \\ \bar{t}_r = t_r - d_{r,IF}/c \\ \bar{N}_{r,1}^s = N_{r,1}^s + B_{r,1} - B_1^s + \left(d_{r,IF} - d_{IF}^s - \gamma_1\beta_{12}DCB_{r,12} + \gamma_1\beta_{12}DCB_{12}^s\right)/\lambda_1 \\ \bar{N}_{r,2}^s = N_{r,2}^s + B_{r,2} - B_2^s + \left(d_{r,IF} - d_{IF}^s - \gamma_2\beta_{12}DCB_{r,12} + \gamma_2\beta_{12}DCB_{12}^s\right)/\lambda_2 \\ \bar{N}_{r,3}^s = N_{r,3}^s + B_{r,3} - B_3^s + \left(d_{r,IF} - d_{IF}^s - \gamma_3\beta_{12}DCB_{r,12} + \gamma_3\beta_{12}DCB_{12}^s\right)/\lambda_3 \\ IFB_r^s = d_{r,IF} - d_{IF}^s + \gamma_3\beta_{12}\left(DCB_{r,12} - DCB_{12}^s\right) + b_{r,3} - b_3^s \end{cases} \tag{9}$$

$$\alpha_{12} = f_1^2/\left(f_1^2 - f_2^2\right), \quad \beta_{12} = -f_2^2/\left(f_1^2 - f_2^2\right) \tag{10}$$

$$DCB_{r,12} = b_{r,1} - b_{r,2}, \quad DCB_{12}^s = b_1^s - b_2^s \tag{11}$$

$$d_{r,IF} = a_{12}b_{r,1} + \beta_{12}b_{r,2}, \quad d_{IF}^s = a_{12}b_1^s + \beta_{12}b_2^s \tag{12}$$

where $\bar{\rho}_r^s$ is the geometric distance with satellite orbit and clock offset fixed using the IGS precise product; α_{12} and β_{12} are the frequency factors of IF combination; $DCB_{r,12}$ and DCB_{12}^s refer to the differential code bias (DCB) between P1/P2 signals at the receiver and satellite end, respectively; $d_{r,IF}$ and d_{IF}^s is the IF pseudorange hardware delay at receiver side and satellite side, respectively.

It should be noted that, when the dual-frequency satellite and receiver DCB corrections are available, we can correct them for the observables to get the un-biased ionosphere delay parameter. In fact, the receiver DCB is often unknown for most stations, especially in real-time applications. However, the satellite and receiver DCBs are commonly assumed to be a constant for several days (Arikan et al. 2008; Ren et al. 2016). Hence, they can be fully absorbed by the ionosphere and ambiguity parameters and do not impact the position estimation (Chen et al. 2015). In our PPP model, we add an extra code bias parameter for the B3 pseudorange observables for each satellite. All the estimated parameters in our PPP models include:

$$X = [x, y, z, \bar{t}_r, zwd, \bar{I}_{r,1}^s, IFB_r^s, \bar{N}_{r,1}^s, \bar{N}_{r,2}^s, \bar{N}_{r,3}^s] \tag{13}$$

2.2 Stochastic models

The ambiguity parameters and static position coordinates are considered as constants. In kinematic mode, the kinematic position coordinates are modelled as white noise. The clock parameter is normally treated as an epoch-wise parameter for a single-system PPP. For the Kalman filter, the spectral density value for the ZWD parameter is empirically set to $10^{-8}\text{m}^2\text{/s}$. The global mapping functions (Boehm et al.

2006) can be used to project the slant dry and wet delays to the zenith delays. We estimated the ionosphere parameter as a random walk, with a spectral density value of $10^{-4}\text{m}^2/\text{s}$.

The proper weighting of the carrier phase and pseudo-range observations is also an important factor to improve the estimation accuracy. It is known that low elevation observations are generally more susceptible to multipath effects and atmospheric refraction than those at high elevations, thus affecting the quality of the solutions. The elevation-dependent weighting of observations was applied in this research to mitigate the effects of multipath, as well as atmospheric errors. Under the assumption that there are no correlations among B1/B2/B3 observables, the stochastic models of the raw PPP can be expressed as:

$$\sum{}_{UC} = \begin{bmatrix} \sigma_1^2 & 0 & 0 \\ 0 & \sigma_2^2 & 0 \\ 0 & 0 & \sigma_3^2 \end{bmatrix} \tag{14}$$

where $\sigma^2 = a^2 + a^2/\sin^2(el)$; for B1/B2 carrier phase, a is set to be 3mm for IGSO+MEO while 10 mm for GEO; el is the elevation angle of the satellite (unit: rad). The relative weighting of code and carrier phase observations was chosen as $1/10^4$.

As to the stochastic models for the third-frequency observations, Li et al (2017a), Pan et al (2017) reported that the IFCB, i.e., the difference between the current clock products computed with L1/L2 and the satellite clocks computed with L1/L5, was noticed for the new L5 signal provided by the GPS Block IIF satellites. Consequently, the L1/L2 clock products cannot be directly used for L1/L5 PPP. Instead, the IFCB should be estimated with a high accuracy in advance. For BDS system, Guo et al (2016) assumed the same a priori noise in all three carriers, and obtained a similar performance (convergence time and positioning accuracy) for triple-frequency and dual-frequency BDS PPP tests. They did not have a discussion on whether the IFCB exists in the BDS B1/B2/B3 observables when using the B1/B2 satellite clocks products. Zhang et al (2017) investigated the IFCB for GPS Block IIF, Galileo, Beidou-2 and -3. Their findings indicated that the IFCBs for Beidou-2 IGSO+MEO satellites are insignificant except for C06.

We further assess the IFCB magnitude for Beidou-2 IGSO+MEO based on the carrier phase and pseudo-range residual results for BDS triple-frequency PPP. The 'GBM' multi-GNSS precise satellite clock and orbit provided by GFZ is used for PPP solutions. Figure 1 below shows the GPS and BDS residuals for the first and third frequency observables for station ESPA on DOY 100, 2017. The carrier phase residual results show that there is nearly no obvious 'inconsistency' between B3 and B1/B2 observables in our raw PPP model. Hence, it is feasible to perform BDS triple-frequency PPP with current GBM precise products. For GPS, large systematic residuals over than 1 dm are observed for the L5 carrier phase which reflects the existence of GPS IFCB. It is likely that a new set of precise products corresponding to raw observables could be generated to produce a better solution with the raw PPP

model. However, it is another research topic in the future. Considering that no precise PCO/PCV information provided currently for B3 frequency but using the PCO/PCV for B2 for correction, we set the weight ratio for B1/B2/B3 as 4:4:1.
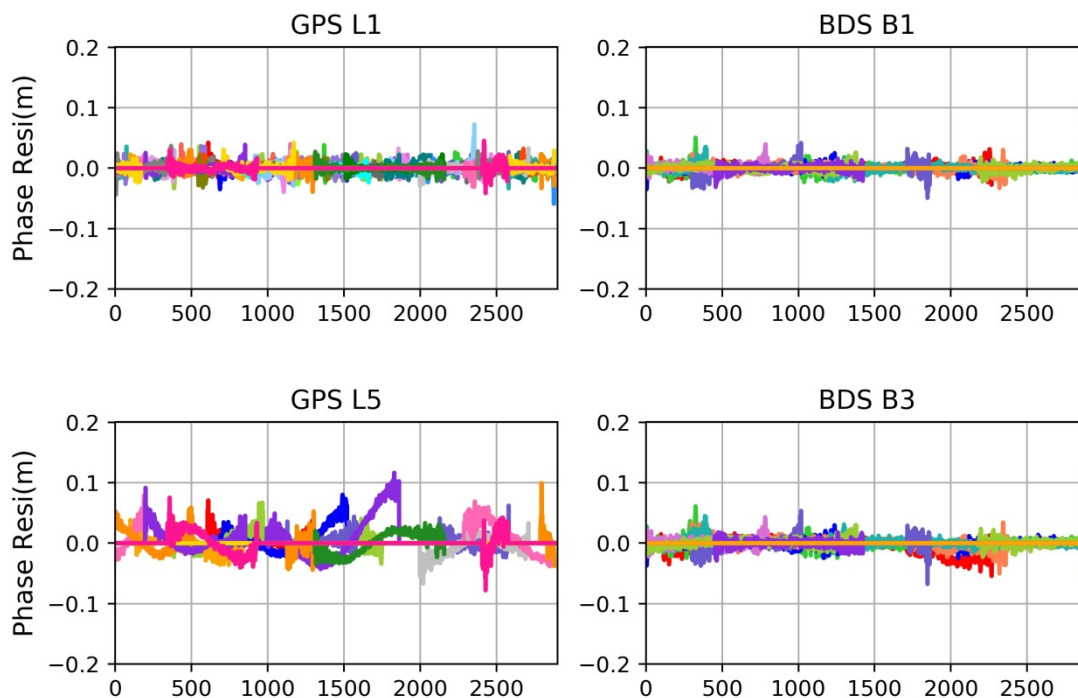

Fig 1. Residual distribution for GPS L1 (left-upper) and L5 (left-lower) carrier phase, BDS B1 (right-upper) and B3 (right-lower) carrier phase.

2.3 Raw UPD estimation and triple-frequency PPP AR

In our raw PPP model, there exists high correlation among the raw triple-frequency ambiguity and the ionosphere parameter. It means that the raw float ambiguity may have a relatively low accuracy for UPD estimation. A very popular approach to ambiguity resolution is to form linear combinations of observations or parameters to mitigate the presence of some error sources, such as geometric or ionospheric errors. The created linear combinations of ambiguities (such as wide-lane ambiguity) would have better precision and are less correlated than the original ambiguities. Generally, they are corresponding to the combined carrier phase which has a relatively long wavelength and is less sensitive to the ionosphere error. This is typically done using a Z-transformation matrix from the LAMBDA method. The LAMBDA method creates linear combinations based on the measurement precision, the frequency number, the structure of the mathematical model employed, for instance the receiver-satellite geometry.

Based on the data processing results, we found that for most cases, after decorrelation, the first two integer linear combinations which have the smallest estimation standard deviation are often [0, 1, -1] and [1, -1, 0]. The third best integer

linear combinations probably are [4, -3, 0], or [3, -4, 2]. These linear combinations can be characterized by low noise and long wave-lengths. Hence, for a continuous arc without cycle slip, the decorrelated ambiguity estimates can be further formulated as:

$$\begin{bmatrix} R^s_{r,1} \\ R^s_{r,2} \\ R^s_{r,3} \end{bmatrix} = \begin{bmatrix} x^s_{r,1} & x^s_{r,2} & x^s_{r,3} & -x^s_{r,1} & -x^s_{r,2} & -x^s_{r,2} \\ y^s_{r,1} & y^s_{r,2} & y^s_{r,3} & -y^s_{r,1} & -y^s_{r,2} & -y^s_{r,3} \\ z^s_{r,1} & z^s_{r,2} & z^s_{r,3} & -z^s_{r,1} & -z^s_{r,2} & -z^s_{r,3} \end{bmatrix} \begin{bmatrix} u_{r,1} \\ u_{r,2} \\ u_{r,3} \\ u^s_1 \\ u^s_2 \\ u^s_3 \end{bmatrix} \tag{15}$$

where $R^s_{r,j}$ is the fractional part of $j\text{-}th$ linear combination of the raw ambiguities, $x^s_{r,j}, y^s_{r,j}\ z^s_{r,j}$ is the coefficient corresponding to the UPD at B1, B2 and B3 frequency, respectively, and u^j_r, $u^{s,j}$ denote receiver and satellite UPDs.

Assume that m satellites have been tracking in a network of n stations, the undifferenced ambiguity in each continuous arc can be put together to form a set of equations in the form of (15). In order to eliminate the rank deficiency, the UPD of the satellite which is observed by most stations are fixed to zero (Zhang and Li 2013). Hence, the following constraints are introduced into the equation set to estimate the single-differenced between satellite raw UPD for other satellites.

$$0 = u^s_j, \quad j = (1,2,3) \tag{16}$$

A least-squares approach is applied to estimate the satellite UPDs. We would eliminate the input ambiguities with a high formal sigma or small number of observations and down-weight the float ambiguity with a large residual during the iterative process. The least-square method is executed iteratively until there are no float ambiguity would be down-weighted.

The traditional PPP AR at user end is conducted in two sequential steps. First, the WL ambiguities from Melbourne-Wübbena (MW) combination observable (Melbourne 1985; Wübbena 1985) are corrected with WL UPDs and aimed to be fixed by rounding. If WL ambiguities are successfully fixed, then, the NL ambiguities are derived and corrected with NL UPDs. A search strategy based on the LAMBDA method (Teunissen 1995) is applied to search for the optimal integer solution for NL integer ambiguities.

Different from the traditional PPP AR strategy, we do not need to employ the geometry-free and ionosphere-free MW combination based on measurements on L1/L2 or L2/L5 frequency to perform WL or EWL AR at user end. The accuracy of WL ambiguity derived from MW combinations could be decreased by the large pseudo-range measurement noise and multipath. Instead, the single-differenced ambiguities between satellites for each frequency are directly formed with the raw

ambiguity estimation from the raw PPP model. With UPDs corrected, the estimators and variance-covariance matrix of single-differenced ambiguities are feed into the LAMBDA algorithm to search for the correct integer solution. In the cases that the full vector of integer ambiguities cannot be resolved with a sufficiently high success rate, we employ the method proposed by Li and Zhang (2015) to try to fix a subset of ambiguities. In the preprocessing stage for PPP AR, the ambiguity with large standard deviation (over than 0.8 cycles) or low elevation (<10 degrees) or small continuous epoch lock count (<8) would be rejected for fixing in order to speed up the PAR.

3 Experiment analysis

The BDS observations, recorded at 30s sampling intervals from IGS MGEX, were used to validate the effectiveness of the triple-frequency UPD estimation and PPP AR method based on raw PPP model. Figure 2 shows the distribution of the GPS+BDS reference network and user stations. 95 stations were used for UPD estimation of which about 35 stations denoted by the green circles provide B1/B2/B3 triple-frequency observables. 10 stations denoted by red stars were used for the PPP tests. The daily observations from DOY 100 to 120, 2017, were used in this study. At the user end, daily observables were separated into 16 1.5-hour-long observable sessions for experiments. The 1.5-hour-long observable was removed if its average visible BDS IGSO+MEO satellite is less than 5. In total there were about 2700 tests finally used for experiments. Site information for user stations, including the site name, receiver type, antenna type, and average visible satellite number per epoch (AVS), were summarized in Table 1.

Table 1 Site information of ten user stations. The information includes the name, receiver type, antenna type, average visible satellite number per epoch (AVS) of BDS IGSO+MEO.

Site Name	Rec Type	Ant Type	AVS (BDS IGSO+MEO)
ARUB	SEPT POLARX5	LEIAR25.R3 NONE	5.7
CUT0	TRIMBLE NETR9	TRM59800.00 SCIS	5.7
ESPA	TRIMBLE NETR9	JAVRINGANT_DM SCIS	5.6
KARR	TRIMBLE NETR9	TRM59800.00 NONE	6.4
KAT1	SEPT POLARX5	LEIAR25.R3 LEIT	6.7
LURA	TRIMBLE NETR9	TRM59800.00 NONE	6.2
MCHL	TRIMBLE NETR9	TRM59800.00 NONE	5.6
MRO1	TRIMBLE NETR9	TRM59800.00 NONE	6.0
PARK	TRIMBLE NETR9	ASH701945C_M NONE	5.1
XMIS	TRIMBLE NETR9	JAVRINGANT_DM NONE	6.8

The combined precise GPS and BDS satellite orbit and clock products provided by GFZ (Deng et al. 2014) were used, and the corresponding UPD products were estimated and employed for the PPP AR tests. We applied the absolute antenna phase centres model and the phase wind-up corrections (Wu et al. 1993). To maintain

consistency with the GBM precise products, the satellite PCO+PCV corrections estimated by ESA were applied for BDS while "igs14.atx" were used for GPS PCO+PCV corrections (Rebischung et al. 2016). Because the receiver PCO and PCV corrections for BDS signals were not available at this time, we simply used GPS corrections for BDS signals, which was consistent with the strategy for BDS precise orbit determination and clock estimation (Lou et al. 2014; Li et al. 2015). In addition, for the B3 frequency observables, the PCO and PCV corrections for the B2 frequency were used. The elevation-dependent BDS satellite-induced code biases were corrected according to Wanninger and Beer (2015). The elevation cut-off angle was set to 10 degrees.

Three groups of BDS PPP solutions were performed and compared: triple-frequency ambiguity-float PPP (solution A), triple-frequency PPP but only tried to fix B1/B2 ambiguities (solution B), and triple-frequency PPP with B1/B2/B3 AR (solution C). We validated the integer ambiguity solutions using two popular indices: the bootstrapping success rate and the ratio-test (Ji et al. 2010). Only when the requirement of the success rate (0.99) and the ratio test (3.0) has been satisfied, the integer ambiguities would be accepted.
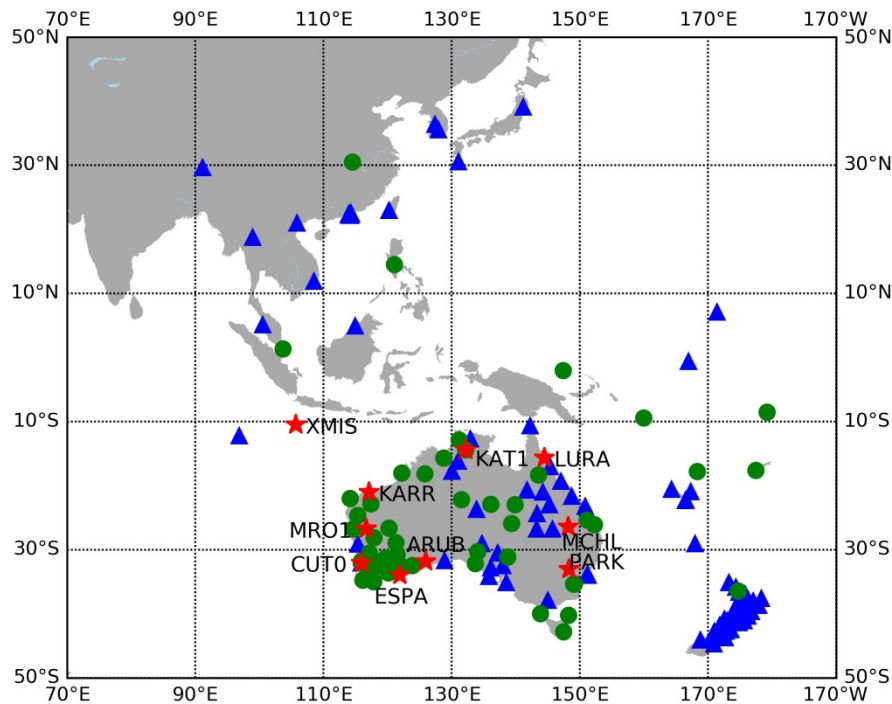

Fig 2. Distribution of the BDS reference network and user stations. The blue triangles denote the reference stations with dual-frequency BDS observables while the green circles denote those with triple-frequency BDS observables; the red stars denote the user stations for investigating the performance of triple-frequency PPP AR.

3.1 Evaluation of triple-frequency UPD

The accuracy of UPD estimation has a great impact on the ambiguity-fixed PPP

solutions. The posteriori residuals of input float ambiguity from Equation (15) were given in figure 3 to analyse the internal precision indicator for UPD estimates. Both, the residual distributions for the raw and decorrelated ambiguities were shown, with totally 78000 ambiguity input on DOY 115, 2017. The root-mean-square (RMS) of the residuals of the decorrelated ones was 0.08 cycles, while that of the raw residuals was 0.21 cycles. With UPD corrected, about 75000 decorrelated ambiguities closed to the nearest integer within 0.25 cycles, while only 59000 raw ones within 0.25 cycles. This comparison clearly showed that the decorrelated ambiguities had a much higher and better consistency than the original ambiguities. Also it indicated that it is better to fix the integer linear combination of ambiguities with decorrelation.
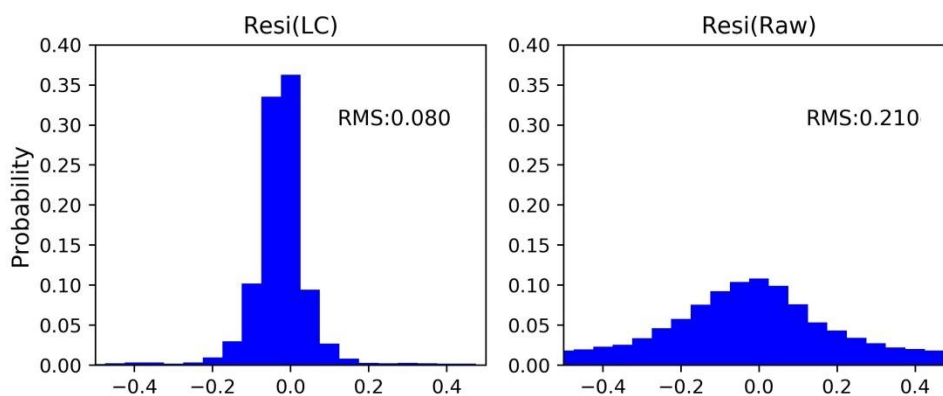

Fig. 3 Distributions of residuals of the linear-combination (left panel) and raw (right panel) ambiguity bias (cycle). The residual is the difference between the input float ambiguity used for UPD estimation and the calculated ambiguity with the final UPD estimates and the integer part of the ambiguity.
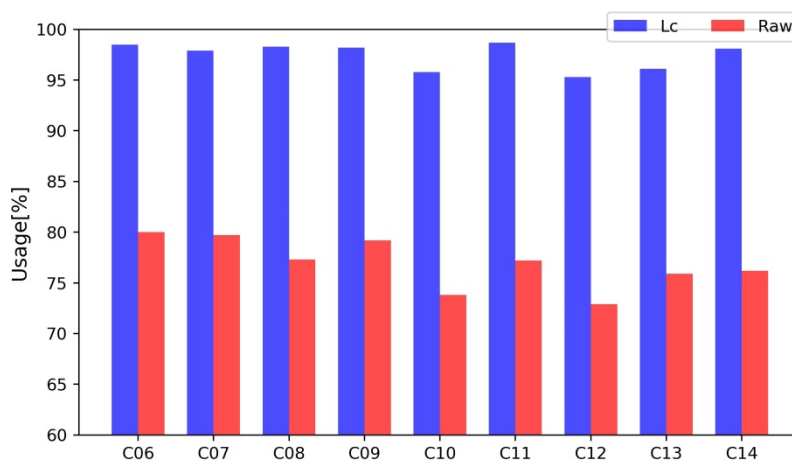

Fig. 4 Usage rate of the BDS float ambiguities at raw frequency and linear combination.

The usage rate of triple-frequency BDS UPD, that is, the percentage of the number of input ambiguities finally contributed to UPD estimation among all the input float ambiguities, was also assessed. Figure 4 shows the average usage rate of

both linear-combination ambiguity and raw ambiguity for each BDS IGSO+MEO satellite. As shown in Figure 4, the minimum and maximum usage rate reached 95.3% and 98.7%, respectively, which means almost all of the decorrelated BDS ambiguities were used for UPD estimation. These results were close to the usage of BDS NL ambiguities, however, much higher than the usage of BDS WL ambiguities reported by Li et al. (2017b). This is reasonable since the linear combination ambiguity in this study and the NL ambiguities in Li et al (2017b) were mainly derived from carrier-phase measurements over a long period with a much larger weight compared to code observations. However, in the study of Li et al (2017b), the WL ambiguities derived from the MW-combination were seriously affected by BDS code biases and code measurement errors. Nevertheless, the usage for the raw float ambiguity was much lower than that of linear combination ambiguity. The minimum, maximum and average usage rates were 72.9, 80.0 and 76.9%, respectively.
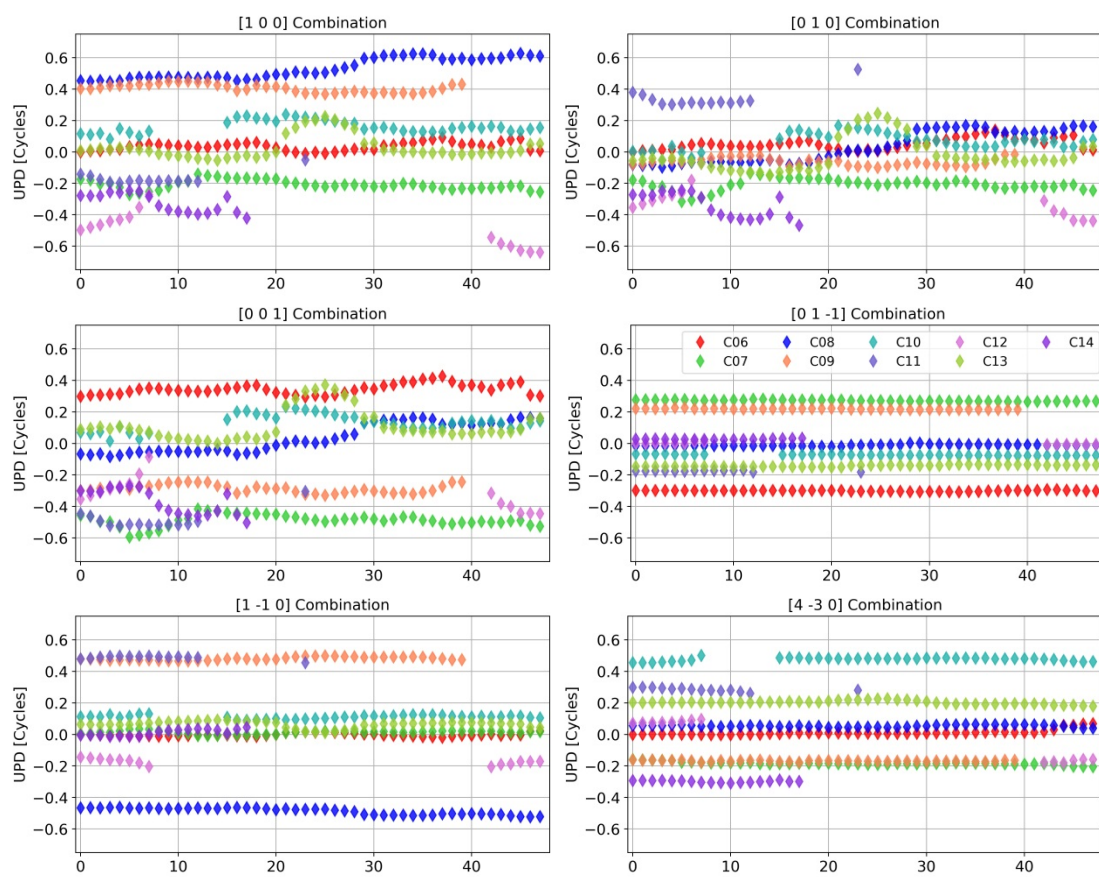

Fig 5 Time series of the raw and linear-combination BDS UPD in each 30 min session, on 30 April, 2017

Furthermore, figure 5 shows the time series of BDS UPDs in each 30 min session, on 30 April, 2017. For the UPD at raw frequency, it was found that generally, the daily variation of raw UPD is about 0.25 cycles for C06-C10. The daily variation of C11-C14 was a little larger than that of IGSO satellites, probably caused by the worse

13

satellite visibility. The UPD variation between adjacent sessions was about 0.05-0.08 cycles. For all BDS IGSO+MEO satellites, the daily variation of EWL, WL, [4, -3, 0] linear combination UPDs was less than 0.03, 0.06 and 0.07 cycles. The variations of linear combination UPD between adjacent sessions were generally less than 0.03 cycles. These results indicate that three groups of BDS UPD linear combination can be estimated on a daily basis and can even be predicted for real-time applications with an update time interval of several days for the Asia-Pacific region.

3.2 Positioning accuracy comparison

The positioning accuracy information of 1.5h static PPP AR for each station over all test days is given in Table 2. One can see that currently BDS static PPP with 1.5h observation can only achieve an accuracy of 5-10 centimetres in east, 3-5 cm in north and 7-11cm in vertical component, respectively. These accuracies were much better than those reported by Li et al (2017b) due to the fact that we only selected the session data whose average IGSO+MEO satellite number is more than 4 in this study while in Li et al (2017b) there were lots of session data which only recorded a few BDS IGSO+MEO (less than 5 on average). In addition, the time length of one session data is 0.5h longer than that used in Li et al (2017b). We can see that the averaged positioning bias of CUT0, ESPA and KAT1 were slightly smaller than those of the other seven stations. This is probably attributed to the fact that these three stations have a little better data quality with the multipath-resistant GNSS antenna installed. The RMS of all 1.5h solutions was improved significantly by AR. With triple-frequency AR, the highest positioning accuracy of (4.7, 3.3, 7.2) centimetres in the east, north and up directions, respectively, was achieved by solution C. Triple-frequency PPP AR improved the positioning accuracy by 37.3, 19.5 and 22.4% compared with solution A, while 16.6, 10.0 and 11.1% compared with solution B, in the east, north and up directions, respectively.

Table 2 The averaged positioning bias with 1.5 hour observation for each test stations.

SITE	Solution A			Solution B			Solution C		
	E	N	U	E	N	U	E	N	U
ARUB	7.2	4.7	9.1	5.3	4.2	8.1	4.3	3.7	6.9
CUT0	6.6	3.7	8.4	4.4	3.0	7.1	3.4	2.7	5.7
ESPA	6.3	3.5	8.1	4.1	3.2	6.9	3.1	2.9	5.9
KARR	7.9	4.0	8.8	4.6	3.8	8.1	4.0	3.5	7.6
KAT1	7.1	3.5	8.2	4.2	3.3	6.8	3.3	2.9	6.0
LURA	7.7	4.5	10.8	6.9	3.9	8.9	5.8	3.4	7.8
MCHL	6.5	3.9	9.4	4.8	3.3	8.6	4.0	3.1	8.1
MRO1	9.4	4.0	9.7	7.8	3.8	8.9	7.0	3.6	7.9
PARK	8.2	3.9	10.1	7.3	3.5	8.9	6.1	3.3	8.2
XMIS	9.4	5.0	10.5	8.4	4.4	9.1	7.2	3.7	8.3
Average	7.6	4.1	9.3	5.7	3.6	8.1	4.7	3.3	7.2

In order to further analyse the benefit of triple-frequency observation on the positioning accuracy of PPP AR, the results of one example which can fix comparable number of epoch for dual-frequency and triple-frequency AR, and the other one which can only fix enough epoch in triple-frequency PPP AR are presented in figure 6 and 7, respectively, for a further discussion.

Figure 6 shows one typical 3D bias for three PPP solutions, taking the results with observations between 04:00 and 06:00 from station CUT0, on DOY 108, 2017, as example. Solution C succeeded in fixing BDS PPP ambiguities from the 13-th epoch and obtained an epoch fixing rate of 93.3%. While solution B took 49 epochs to achieve the first ambiguity fixing and obtained an epoch fixing rate of 73.4%. For this sample, it could fix comparable number of epoch for dual-frequency and triple-frequency AR. Nearly the same 3D positioning accuracy was achieved for solutions B and C (3.2 and 2.9 cm, respectively). The insignificant difference of 3D positioning bias revealed that in the case that dual-frequency PPP ambiguity can be successfully fixed continuously, triple-frequency PPP AR had only marginal improvement on position accuracy. Due to the lack of precise PCO/PCV corrections on the B3 frequency, we have down-weighted the B3 observations. This may lead to the insignificant contribution of triple-frequency PPP AR on positioning accuracy. In addition, for ambiguity-float BDS PPP, Guo et al (2016) has reported similar conclusion on the contribution on positioning accuracy with additional third-frequency observations. A comprehensive study on the contribution of additional B3 observation on PPP AR is still needed in the future when BDS-3 is in fully operation with global service and BDS-related precise products and error models have been well improved.
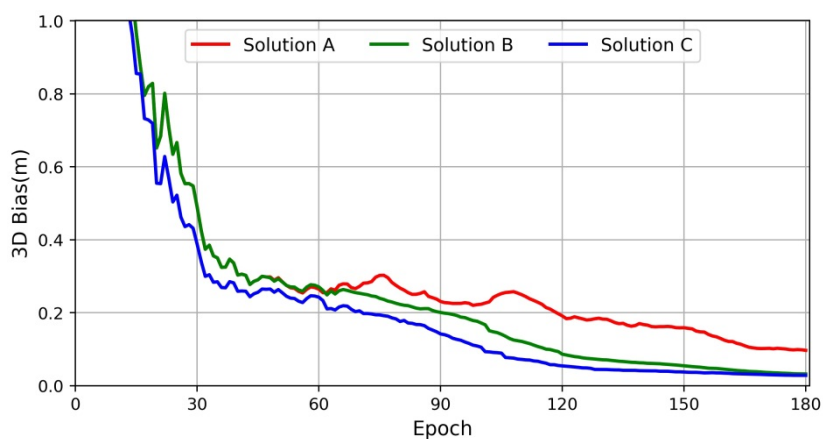

Fig. 6 The 3D bias time series for three groups of PPP solutions with observations between 04:30 and 06:00 at station CUT0, on DOY 108, 2017.
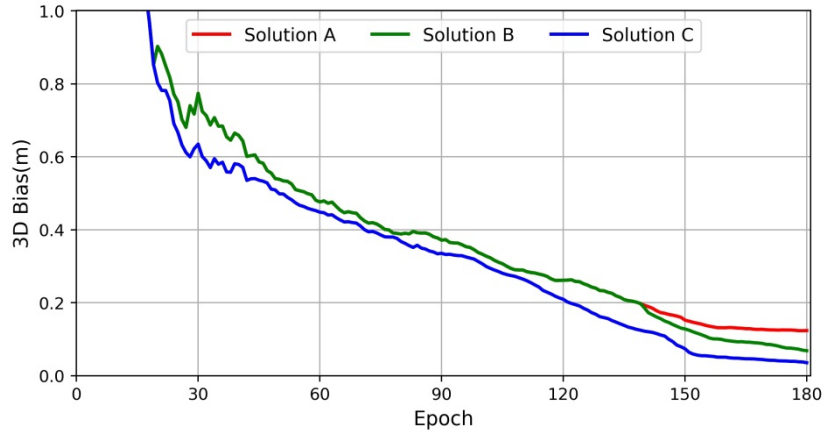
Fig. 7 The 3D bias time series for three groups of PPP solutions with observations between 12:00 and 13:30 at station MCHL, on DOY 106, 2017.

Figure 7 shows the other typical 3D bias for three PPP solutions, taking the results with observations between 12:00 and 13:30 from station MCHL, on DOY 106, 2017, as example. For this sample, it was difficult to fix dual-frequency PPP ambiguity for most epochs. Solution B took 140 epochs to achieve the first ambiguity fixing and obtained an epoch fixing rate of 22.7%. Nevertheless, due to the fact that more triple-frequency ambiguity linear combination, such as EWL, WL, [1, 4, -5], with higher precision can be formed, it was much easier to fix triple-frequency PPP ambiguity for many epochs. Solution C succeeded in fixing BDS PPP ambiguities from 21-th epoch and obtained an epoch fixing rate of 89.0%. The final 3D positioning bias was 12.3, 6.9 and 3.2 cm for solution A, B and C, respectively. From these results, it can be concluded that the additional observations from the third frequency can improve the AR availability for BDS PPP, especially under constraint environments when the dual-frequency PPP AR are limited.

3.3 Convergence time comparison

Another crucial performance indicator of PPP is the convergence time. We calculated the quadratic mean positioning bias for each epoch with all tests. These biases series indicating the average convergence series is shown in figure 8. It can be seen that solution B can achieve successful dual-frequency PPP AR and begun to accelerate the convergence when the horizontal and vertical positioning bias of ambiguity-float PPP was about 3 dm. As for solution C, triple-frequency PPP AR would accelerate the convergence when the horizontal and vertical positioning bias of ambiguity-float PPP was about 4 and 5 dm, respectively. Generally, with an initialization time of about 8 and 15 minutes, respectively, the position estimation could be improved by AR for solution B and C. It is clear that the overall initialization time was significantly reduced by introducing ambiguity-fixing for both horizontal and vertical directions.
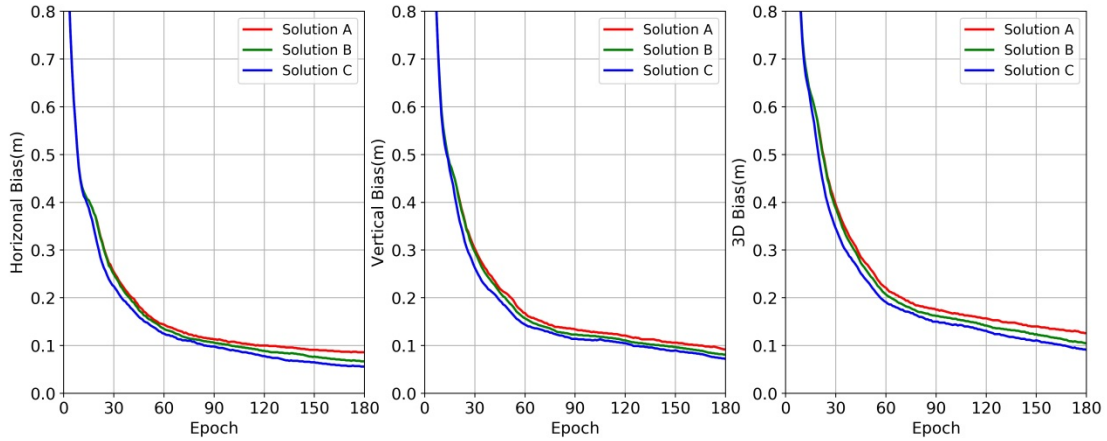
Fig. 8 The average convergence series of BDS PPP for DOY 100-120, 2017 over a 3-h pass of the horizontal (left panel), vertical (middle panel) and 3D component (right panel).

Furthermore, we specify the convergence to be defined as the time required to attain a quadratic mean positioning bias less than 20 cm in 3D component. The solution was required to have a 3D bias of less than 20 cm for 10 epochs for convergence to be attained. Note that when the solution cannot be converged within 90 minutes, the convergence time (CT) would be recorded as 90 minutes. The sessions whose CT was 90 min accounted for 7.9, 5.0 and 4.2% for solution A, B, C, respectively. Still, there were a few cases, which had a little longer convergence time in ambiguity-fixed PPP. This is probably caused by low-quality and accuracy of the session UPD used. Nevertheless, these instances only accounted for 4.8%.
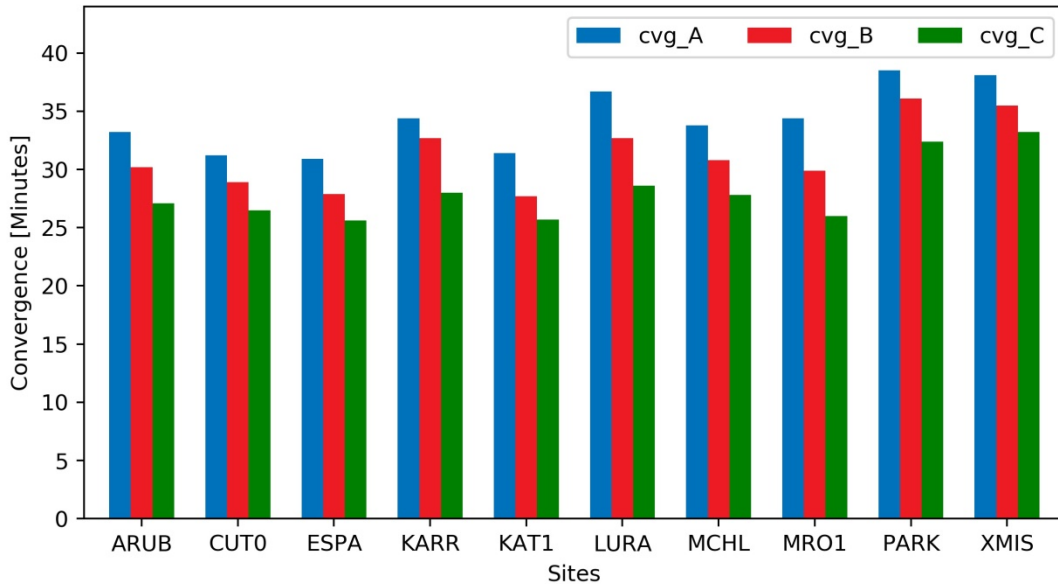

Fig. 9 Average convergence time for solution A, B and C at each station.

Figure 9 presents the average convergence time result for each test station. We also found that the CT of stations CUT0, ESPA, and KAT1 were a little shorter than

17

that of the other stations, for all three groups of solutions. This was maybe because that with the multipath-resistant GNSS antenna installed the BDS data quality collected by these three stations was relatively better than that of the other stations. Among the three groups of solutions, the triple-frequency ambiguity-fixed BDS PPP achieved the fastest CT. The statistical results of all convergence time were as follows: 34.1 min for solution A, 31.0 min for solution B while 27.9 min for solution C. With triple-frequency BDS PPP AR, the average convergence time was reduced by 18.1% compared with solution A, and 10.0% compared with solution B.

4 Conclusions and Remarks

This study proposes a unified UPD estimation and PPP AR method suitable for dual-, triple- and multi- frequency data processing based on a raw GNSS model. The UPDs on each frequency are directly estimated with the raw float ambiguities derived from both dual- and three- frequency observables and can be used for resolving full or partial ambiguities easiest to be fixed. The treatment of BDS raw triple-frequency UPD estimation is provided in details. An important advantage of this model is that it can be extended to the n-frequency (n>=2) case very easily.

With the BDS observables provided by IGS-MGEX, numerous experimental results show that successful triple-frequency BDS UPD estimation and PPP AR can be conducted, with a significant improvement on positioning biases and convergence time, compared with triple-frequency ambiguity-float PPP. In addition, compared with dual-frequency AR, additional the third frequency could contribute to improving the position estimations during the initialization phase and under constraint environments when the dual-frequency PPP AR are limited by a low satellite number. The statistical results demonstrated that an averaged positioning bias of (4.7, 3.3, 7.2) centimetres in the east, north and up directions, respectively, and an averaged 3D convergence time of 27.9 min can be produced by triple-frequency PPP AR. Triple-frequency PPP AR improved the positioning accuracy by 37.3, 19.5 and 22.4% compared with triple-frequency ambiguity-float PPP, while 16.6, 10.0 and 11.1% compared with dual-frequency PPP AR, in the east, north and up directions, respectively. Triple-frequency PPP AR reduced the average convergence time by 18.1% compared with triple-frequency ambiguity-float PPP, and 10.0% compared with dual-frequency PPP AR.

Currently, the performance of BDS triple-frequency PPP AR is still limited by several factors, including: (a). the smaller number of BDS IGSO+MEO satellites and the unbalanced coverage of the BDS constellation. Generally, there are only about 5-6 BDS IGSO+MEO satellites that can be observed and used for AR. The few satellite number and poor spatial geometry condition negatively affected the performance of BDS PPP AR, for both dual- and triple- frequency model; (b). the lack of precise BDS PCO+PCV corrections for the triple-frequency observables and for the receivers end. It would introduce systematic errors to the observable equations. Although its impact can be mitigated by down-weighting the B3 observables, the contribution of the third-frequency observables to the PPP AR is also weakened.

BDS UPD estimates and PPP AR are expected to be refined when a more precise error correction model for BDS is proposed and when more BDS satellites come into service. In addition, the effectiveness of the proposed PPP AR method is expected to be validated employing Galileo observation with four frequencies.

Acknowledgments

References

Arikan F, Nayir H, Sezen U, Arikan O (2008) Estimation of Single Station Interfrequency Receiver Bias Using GPS-TEC. Radio Science, 43, RS4004.

Banville S (2016) Glonass ionosphere-free ambiguity resolution for precise point positioning. J Geod. 90 (5) : 487-496

Boehm J, Niell A, Tregoning P, Schuh H (2006) Global Mapping Functions (GMF): a new empirical mapping function based on numerical weather model data. Geophys. Res. Lett. 33, L07304, http://dx.doi.org/10.1029/2005GL025546, 2006.

Chen JP, Zhang YZ, Wang JG, Yang SN, Dong DN, Wang JX, Qu WJ, Wu B (2015) A simplified and unified model of multi-GNSS precise point positioning. Advances in Space Research. 55 (1): 125-134.

Collins P, Lahaye F, Héroux P, Bisnath S (2008) Precise point positioning with ambiguity resolution using the decoupled clock model. Proc. ION GNSS 2008, Institute of Navigation, Savannah, Georgia, 1315-1322

deLacy MC, Reguzzoni M, Sanso` F (2012) Real-time cycle slip detection in triple-frequency GNSS. GPS Solut 16(3):353-362

Deng Z, Zhao Q, Springer T, Prange L, Uhlemann M (2014) Orbit and Clock Determination-BeiDou, IGS workshop, Pasadena, USA, 23.06-27.06.2014

Deo M, El-Mowafy A (2016) Triple-frequency GNSS models for PPP with float ambiguity estimation: performance comparison using GPS. Survey Review doi:10.1080/00396265.2016.1263179

Elsobeiey M (2015) Precise point positioning using triple-frequency GPS measurements. J Navig 68:480-492.

Forssell B, Martin-Neira M, Harris RA (1997) Carrier phase ambiguity resolution in GNSS-2. In: Proc. ION GPS-1997, Institute of Navigation, Kansas City, Missouri, Sept, pp 1727-1736

Ge M, Gendt G, Rothacher M, Shi C, Liu J (2008) Resolution of GPS carrier-phase ambiguities in Precise Point Positioning (PPP) with daily observations. J Geod 82(7):389-399

Geng J, Bock Y (2013) Triple-frequency GPS precise point positioning with rapid ambiguity resolution. J Geod 87(5):449-460

Geng J, Shi C (2017) Rapid initialization of real-time PPP by resolving undifferenced

GPS and GLONASS ambiguities simultaneously. J Geod 91(4):361–374

Gu SF, Lou YD, Shi C, Liu JN (2015) BeiDou phase bias estimation and its application in precise point positioning with triple-frequency observable. J Geod. 89 (10):979-992

Guo F, Zhang XH, Wang JL (2015) Timing group delay and differential code bias corrections for BeiDou positioning. J Geod 89(5):427-445

Guo F, Zhang XH, Wang JL, Ren XD (2016) Modeling and assessment of triple-frequency BDS precise point positioning. J Geod 90(11):1223-1235

Ji S, Chen W, Ding X, Chen Y, Zhao C, Hu C (2010) Ambiguity validation with combined ratio test and ellipsoidal integer aperture estimator. J Geod 84(10): 597-604

Kouba J, Héroux P (2001) Precise point positioning using IGS orbits and clock products. GPS Solut 5(2): 12-28

Laurichesse D, Mercier F, Berthias JP, Broca P, Cerri L (2009) Integer ambiguity resolution on undifferenced GPS phase measurements and its application to PPP and satellite precise orbit determination. Navigation 56(2):135-149

Li B, Feng Y, Shen Y (2010) Three carrier ambiguity resolution: distance-independent performance demonstrated using semigenerated triple frequency GPS signals. GPS Solut 14(2):177-184.

Li H, Li B, Lou L, Yang L, Wang J (2017a) Impact of GPS differential code bias in dual- and triple-frequency positioning and satellite clock estimation. GPS Solut 21 (3): 897-903

Li P, Zhang XH (2015). Precise point positioning with partial ambiguity fixing. Sensors 15(6): 13627-13643

Li P, Zhang XH, Guo F (2017b). Ambiguity resolved precise point positioning with GPS and Beidou. J Geod 91 (1): 25-40

Li X, Ge M, Dai X, Ren X, Fritsche M, Wickert J, Schuh H (2015) Accuracy and reliability of multi-GNSS real-time precise positioning: GPS, GLONASS, BeiDou, and Galileo. J Geod 89 (6): 607-635.

Lou Y, Liu Y, Shi C, Yao XG, Zheng F (2014) Precise orbit determination of BeiDou constellation based on BETS and MGEX network. Sci Rep 4, 4692.

Melbourne WG (1985) The case for ranging in GPS-based geodetic systems. In: Proceedings of the first international symposium on precise positioning with the global positioning system, Rockville, 15–19 April, pp 373–386

Pan L, Zhang X, Li X, Liu Jingnan, Li Xin (2017) Characteristics of inter-frequency clock bias for Block IIF satellites and its effect on triple-frequency GPS precise point positioning. GPS Solut 21(2): 811-822

Petit G and Luzum B (2010) IERS Technical Note No. 36, IERS Conventions 2010, International Earth Rotation and Reference Systems Service, Frankfurt, Germany.

Ren X, Zhang X, Xie W, Zhang K, Yuan Y, Li X (2016) Global ionospheric modelling using multi-GNSS: BeiDou, Galileo, GLONASS and GPS. Sci Rep 6:33499

Rebischung P, Altamimi Z, Ray J, Garayt B (2016) The IGS contribution to ITRF2014. J Geod 90 (7): 611-630

Simsky A (2006) Three's the charm: triple-frequency combinations in future GNSS. InsideGNSS:38-41, July/August

Teunissen PJG (1995) The least-squares ambiguity decorrelation adjustment a method for fast GPS integer ambiguity estimation. J Geod 70(1-2):65-82

Teunissen PJG, Joosten P, Tiberius C (2002) A comparison of TCAR, CIR and LAMBDA GNSS ambiguity resolution. In: Proceedings of the ION GPS-2002, pp 2799–2808, Portland, OR, 24-27 September

Wanninger L, Beer S (2015) BeiDou satellite-induced code pseudorange variations: diagnosis and therapy. GPS Solut 19(4):639-648.

Wu JT, Wu SC, Hajj GA, Bertiger WI, Lichten SM (1993) Effects of antenna orientation on GPS carrier phase. Manuscripta Geodaetica 18(2):91-98

Wubbena G (1985) Software developments for geodetic positioning with GPS using TI-4100 code and carrier measurements. In: Proceedings of first international symposium on precise positioning with the global positioning system, Rockville, 15–19 April, pp 403-412

Zhang X, He X (2016) Performance analysis of triple-frequency ambiguity resolution with BeiDou observations. GPS Solut 20(2):269-281.

Zhang XH, Li P (2013) Assessment of correct fixing rate for precise point positioning ambiguity resolution on global scale. J Geod 87(6):579-589

Zhang XH, Li P (2016) Benefits of the third frequency signal on cycle slip correction. GPS Solut. 20(3): 451-460

Zhang XH, Wu MK, Liu WK, Li XX, Yu S, Lv CX, Wickert Y (2017) Initial assessment of the COMPASS/BeiDou-3: new-generation navigation signals. J Geod: 1-16. doi: 10.1007/s00190-017-1020-3

Zumberge JF, Heflin MB, Jefferson DC, Watkins MM, Webb FH (1997) Precise point positioning for the efficient and robust analysis of GPS data from large networks. J Geophy Res 102(B3):5005-5017